Analogies between the topologial insulator phase of 2D Dirac materials and the superradiant phase of atom-field systems

Manuel Calixto*
Departamento de Matemática Aplicada and Instituto Carlos I de Física Teórica y Computacional (iC1), Facultad de Ciencias, Universidad de Granada, Fuentenueva s/n, 18071 Granada, Spain.

Elvira Romera†
Departamento de Física Atómica, Molecular y Nuclear and Instituto Carlos I de Física Teórica y Computacional (iC1), Universidad de Granada, Fuentenueva s/n, 18071 Granada, Spain.

Octavio Castaños‡
Instituto de Ciencias Nucleares, Universidad Nacional Autónoma de México, Apdo. Postal 70-543, 04510, CDMX, Mexico
(Dated: March 12, 2020)

A semiclassical phase-space perspective of band- and topological-insulator regimes of 2D Dirac materials, and normal- and superradiant-phases of atom-field interacting models is given in terms of delocalization, entropies, and quantum correlation measures. From this point of view, the low-energy limit of tight-binding models describing the electronic band structure of topological 2D Dirac materials like phosphorene and silicene with tunable band gaps, share similarities with Rabi-Dicke and Jaynes-Cummings atom-field interaction models, respectively. In particular, the edge state of 2D Dirac materials in the topological insulator phase exhibits a Schrödinger cat structure similar to the ground state of two-level atoms in a cavity interacting with a one-mode radiation field in the superradiant phase. Delocalization seems to be a common feature of topological insulator and superradiant phases.

PACS numbers: 03.65.Vf, 03.65.Pm,89.70.Cf, 64.70.Tg, 73.43.Nq,
Keywords: Topological insulators, phosphorene, silicene, atom-field interacting models, edge and ground states, tunable band gap, coherent states, Husimi function, phase space, localization and entanglement measures, Schrödinger cat

I. INTRODUCTION

Until quite recently, Landau theory constituted the usual paradigm to describe phase transitions occurring at a critical point of some control parameters. Roughly speaking, this is based on the concept of "order parameter" (related to different organizations of the atoms or particles in the materials) that is finite in a broken symmetry phase. Different orders correspond to different symmetries in the organization of the constituent atoms (liquids, crystals, etc). Gapless excitations (often called Goldstone modes) are a well-known consequence of the spontaneous symmetry breaking of a continuous underlying symmetry; for example, the spontaneous breakdown of the continuous translation symmetry of a liquid to the discrete symmetry of a crystal in solidification.

Landau theory can be generalized to describe quantum phase transitions (QPT), which are driven by quantum fluctuations since they take place at zero temperature. Examples of physical systems undergoing a QPT are: superconductor-insulator transitions, ferromagnets, radiation-matter interaction models, etc [1, 2]. In this article we shall pay attention to paradigmatic atom-field models displaying a superradiant phase above some critical value of the external electric field. For example: Rabi, Dicke, and Jaynes-Cummings (JC) models [3, 4]. The JC model is a theoretical model of great interest to atomic physics, quantum optics, solid-state physics and quantum information circuits, both experimentally and theoretically. It also has applications in coherent control and quantum information processing (see [4] for a recent recent reference reviewing the physics of the JC model). Basically, it describes the system of a two-level atom interacting with a quantized mode of an optical cavity (a bosonic field) that can cause spontaneous emission and absorption. It was originally developed to study the interaction of atoms with the quantized electromagnetic field in order to investigate the phenomena of spontaneous emission and absorption of photons in a cavity.

Investigation of quantum critical phenomena beyond the Landau paradigm leads to topological phase transitions (TPT) which represent a new class of quantum critical phenomena. In fact, it is usually said that TPTs cannot be described within the usual framework of Landau theory because they constitute a new king of order that is beyond the usual symmetry description. Such is the case of chiral spin textures (in high temperature superconductivity) and quantum Hall states with the same symmetry but different "topological order". In this article we shall concentrate on 2D topological insulators (see [5–7] for extensive reviews and [8] for the special case of silicene), which are examples of "symmetry-protected topological

*Electronic address: calixto@ugr.es
†Electronic address: eromera@ugr.es
‡Electronic address: ocasta@nucleares.unam.mx

order" (that respect time-reversal symmetries). Topological insulators have gapless boundary (edge) conducting states that are symmetry protected and dispersionless (robust against impurities and perturbations), similar to quantum Hall effect. We shall concentrate on 2D materials of the graphene family, in particular: silicene and phosphorene. They are two-dimensional allotropes of silicon and black phosphorus, respectively, with a hexagonal honeycomb structure similar to that of graphene but with a buckled structure which gives them a tunable band gap by applying external electric fields. They are also called Dirac materials because their low energy (long wave length) effective electron dynamics can be described by a Dirac equation of electrons moving at the Fermi velocity. Unlike graphene, silicene and phosphorene can develop edge currents due to a non-zero spin-orbit coupling (non-zero Dirac mass gap) which plays the role of an "intrinsic" (versus external) magnetic field (when compared to quantum Hall effect). These edge currents can be controlled by tunning the band gap (Dirac mass) applying a perpendicular electric field to the material sheet, thus inducing transitions from a band (standard) insulator (BI) to a topological (edge conducting) insulator (TI) phase. In general a TI-BI transition is characterized by a band inversion with a level crossing (edge states) at some critical value of a control parameter and, like topological phases, TI and BI phases can be characterized by topological charges like Chern numbers [8]. Their particular structure confers Dirac materials interesting physical properties. In particular, phosphorene is relevant for optical properties and it can be used as a photodetecting material [9]. It also has interest in the framework of field effect transistor applications in nanoelectronics [10–12], because of its direct band gap (up to 2eV) and a high carrier mobility (1000 cm^2 V^{-1} s^{-1}) at room temperature. Phosphorene's electronic devices have been manufactured with considerable success, showing a great performance [13–16].

Although topological and symmetry-breaking (Landau-like) quantum phases are different in nature, one can still identify some similarities between them, and this is one of the purposes of this article. We shall show that an information-theoretical analysis in phase space of topological and standard quantum phases reveals a similar structure around the critical points, specially between edge and ground states. Actually, localization, entropy and entanglement measures of Hamiltonian eigenstates have proven to be good markers of the QPT for the Dike model of matter-radiation interaction [17–20], vibron model of molecules [21–23], the ubiquitous Lipkin-Meshkov-Glick [24–27], Bose-Einstein condensates [28], bilayer quantum Hall effect [29–31], etc. As shown in [32], these entropic measures are even capable of identify the order of the corresponding QPT. Inverse participation ratio and several kinds of entropies have also turned out to be useful to visualize the TI-BI transition in phosphorene [33] and silicene [34–37], where entropy-based Chern-like numbers distinguishing TI and BI phases have been defined. In this article we pay special attention to phosphorene, which has been less explored. We shall see that the low-energy (long wavelength) limit of tight-binding models of phosphorene and silicene share some similarities with traditional Rabi-Dicke and Jaynes-Cummings atom-field interaction models, respectively. There is a clear correspondence between the TI (resp. BI) regime of phosphorene and silicene and the superradiant (resp. normal) quantum phase of Rabi-Dicke and Jaynes-Cummings models. In particular, the edge state of 2D Dirac materials in the topological insulator phase exhibits a Schrödinger cat structure similar to the ground state of atom-field models in the superradiant phase. Therefore, delocalization seems to be a common feature of both kind of phase transitions, and the extensive knowledge on Rabi-Dicke and Jaynes-Cummings models can help to better understand phosphorene and silicene, respectively.

The work is organized as follows. Firstly in section II we introduce the low energy Hamiltonian describing the properties of phosphorene in the presence of electric and magnetic fields, comparing with the better known case of silicene. In section III we solve the eigenvalue problem for these Hamiltonians, numerically for phosphorene and analytically for silicene, computing Landau levels and edge states and classifying them according to their symmetries (namely parity). In section (IV) we introduce coherent states and the so called Husimi function of pure states and reduced density matrices, which allows a visualization of quantum states in phase-space across the TI-BI transition in the vicinity of a critical point. We restrict ourselves in this case to phosphorene (silicene has been analyzed in [34]). In section V we use information measures (moments of the Husimi distribution) which turn out to be good markers and descriptors of the TI-BI transition. In section (VI) we compare phosphorene and silicene with Rabi-Dicke and Jaynes-Cummings spin-boson models using the framework of coherent states. In particular, we show that edge states exhibit a Schrödinger cat structure in the topological insulator phase, similar to the ground state structure of atom-field systems in the superradiant phase. Finally, section VII is devoted to final conclusions.

II. LOW ENERGY MODEL HAMILTONIANS

We shall start discussing the less known case of phosphorene. Phosphorene is a monolayer of black phosphorus, belonging to the group of 2D gapped Dirac materials similar to graphene, which has been synthesized and studied theoretically and experimentally [13, 38–45]. In phosphorene there are sp^3 bonds with two different bond angles (96.34^o and 103.09^o), each atom has two neighbors at 2.224Å and a third one at 2.44Å and, due to these characteristics, it has an orthorhombic structure with a great stability (see Figure 1).

A tight binding model Hamiltonian

$$\tilde{H}_4 = \sum_{\langle i,j \rangle} t_{ij} c_i^\dagger c_j \tag{1}$$

describing the electronic band structure of phosphorene has been proposed by [46], where summation runs over lattice sites, t_{ij} is the transfer energy between sites i and j. It has been shown [46] that it is enough to consider five hopping links $t_1, \ldots, t_5$, like in figure 1, which eventually provide a band gap $E_g = 4t_1 + 2t_2 + 4t_3 + 2t_5$. The term $c_i^\dagger$ (c_i) represents the creation (annihilation) operator of electrons at site i. The unit cell of phosphorene contains four phosphorus atoms: two in the upper layer and two in the lower layer (see figure 1). Therefore, in the momentum representation, the energy dispersion of phosphorene is described by a four-band Hamiltonian (see [47])

$$\tilde{H}_4 = \sum_{\mathbf{k}} c^\dagger(\mathbf{k}) H_4(\mathbf{k}) c(\mathbf{k}), \tag{2}$$

which can be reduced to a two-band model, due to the D_{2h} point group invariance (that is, considering two points, instead of four, per unit cell). Expanding around the Γ point of the Brillouin zone (up to second order in $\mathbf{k}$) and doing a coordinate rotation (for convenience, like in [46, 48]) of the Pauli matrices ($\sigma_x \to \sigma_z, \sigma_y \to \sigma_x$), one obtains the following simplified $\mathbf{k}\cdot\mathbf{p}$ model for phosphorene (we use the same notation as in [48])

$$H_2 = \begin{pmatrix} E_c + \alpha_x k_x^2 + \alpha_y k_y^2 & \gamma k_x \\ \gamma k_x & E_v + \beta_x k_x^2 + \beta_y k_y^2 \end{pmatrix}. \tag{3}$$

This will be our starting point. The hopping parameters are $t_1 = -1.220$eV, $t_2 = 3.665$eV, $t_3 = -0.205$eV, $t_4 = -0.105$eV, $t_5 = -0.055$eV, and the lengths of the unit cell are $a_x = 3.32$Å and $a_y = 4.38$Å. With these values, the conduction and valence energies are $E_c = 0.34$eV and $E_v = -1.18$eV, respectively, so that the energy gap is $E_g = E_c - E_v = 1.52$eV. The off diagonal parameter $\gamma = -5.2305$eVÅ describes the interband coupling between the conduction and valence bands. As in Reference [48], it will be useful to relate the Hamiltonian parameters $\alpha_{x,y}$ and $\beta_{x,y}$ to some effective masses as $\alpha_{x,y} = \hbar^2/(2m_{cx,cy})$ and $\beta_{x,y} = \hbar^2/(2m_{vx,vy})$. For phosphorene, we have $m_{cx} = 0.793m_e, m_{cy} = 0.848m_e, m_{vx} = 1.363m_e$ and $m_{vy} = 1.142m_e$, where m_e denotes the free electron mass.

We introduce a perpendicular magnetic field $\mathbf{B} = (0, 0, B)$ through the minimal substitution $\hat{\mathbf{p}} \to \hat{\mathbf{p}} - e\mathbf{A}$. Taking the Landau gauge $\mathbf{A} = (-By, 0, 0)$ and defining the annihilation (and creation $\hat{a}^\dagger$) operator,

$$\hat{a} = \sqrt{\frac{m_{cy}\omega_c}{2\hbar}} \left(y - y_0 + i \frac{\hat{p}_y}{m_{cy}\omega_c} \right), \tag{4}$$

where $\omega_c = eB/\sqrt{m_{cx}m_{cy}}, y_0 = \ell_B^2 k_x$ and $\ell_B = \sqrt{\hbar/(eB)}$ denote the cyclotron frequency, the center

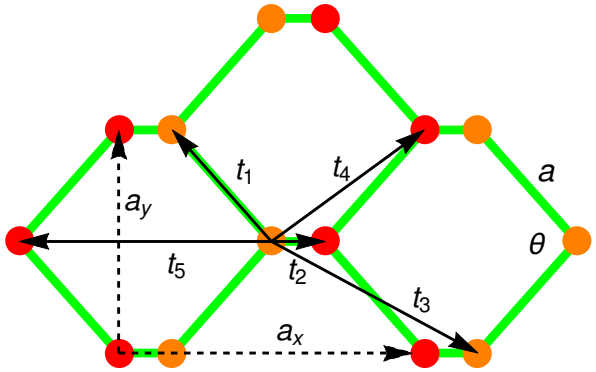

FIG. 1: Top view of phosphorene. Red (orange) balls represent phosphorus atoms in the lower (upper) layer. The in-plane bond length and angle are $a = 2.22$Å and $\theta = 96.79^o$, respectively. The primitive vectors $a_x = 3.32$Å and $a_y = 4.38$Å are denoted by dashed arrows. The first five neighbor hopping sites t_j necessary to describe phosporene [46] are denoted by solid arrows.

and the magnetic length, respectively, the corresponding Hamiltonian adopts the following form

$$\hat{H}_2^B = \hbar\omega_\gamma(\hat{a} + \hat{a}^\dagger)\sigma_x + \frac{E_c + \hbar\omega_c(\hat{a}^\dagger\hat{a} + 1/2)}{2}(\sigma_0 + \sigma_z) + \frac{E_v - \hbar\omega_v(\hat{a}^\dagger\hat{a} + 1/2) - (\hat{a}^2 + \hat{a}^{\dagger 2})\hbar\omega'}{2}(\sigma_0 - \sigma_z), \tag{5}$$

where $\omega_\gamma = \gamma/\sqrt{2}\hbar\ell_B\rho$, $\omega_v = (r_x + r_y)\omega_c$ and $\omega' = (r_x - r_y)\omega_c/2$, with $\rho = (m_{cy}/m_{cx})^{1/4}$, $r_{x,y} = m_{cx,cy}/(2m_{vx,vy})$, σ_x and σ_z are Pauli matrices and σ_0 denotes the two-dimensional identity matrix. In addition to the magnetic field, we shall add an electric field interaction in the usual form $\hat{H}_2^\Delta = \Delta\sigma_z$, with Δ the electric potential. Therefore, our total Hamiltonian for the phosphorene will be

$$\hat{H}_{\rm P} = \hat{H}_2^B + \hat{H}_2^\Delta. \tag{6}$$

The role of the electric field will be to provide a tunable band gap.

Similarly, the low energy regime of a tight-binding model describing the electronic band structure of silicene under a perpendicular magnetic and electric field, is reported by the 2D Dirac Hamiltonian (for simplicity, we restrict ourselves to the linear expansion around the K point of the Brillouin zone, and the fully polarized spin 1/2 case) [49–52]

$$\hat{H}_{\rm S} = \Delta_g\sigma_z + \hbar\omega(\hat{a}\sigma_+ + \hat{a}^\dagger\sigma_-), \tag{7}$$

where $\sigma_\pm = \frac{1}{2}(\sigma_x \pm i\sigma_y)$, $\omega = v\sqrt{2eB/\hbar}$ is the cyclotron frequency ($v = 5 \times 10^5$m/s is the Fermi velocity) and the "Dirac mass" $\Delta_g = \frac{1}{2}\Delta + \frac{1}{2}\Delta_{\rm so}$ provides a band gap, written in terms of the spin-orbit coupling $\Delta_{\rm so} \simeq 4$meV and the electric potential Δ. Later in Section VI, we will comment on some similarities between the phosphorene

$\hat{H}_{\rm P}$ and silicene $\hat{H}_{\rm S}$ low energy Hamiltonians, and the Rabi-Dicke and Jaynes-Cummings models for atom-field interaction, respectively.

III. DIAGONALIZATION: PARITY SYMMETRY, LANDAU LEVELS AND EDGE STATES

Let us denote by $|n,s\rangle$ the basis states of our Hilbert space, with $n=0,1,2,\ldots$, the eigenvalues of $\hat{n}=\hat{a}^\dagger\hat{a}$ and $s=\pm1$ the eigenvalues of σ_z. For convenience, in the following analysis, we are disregarding the degeneracy in k_x due to translational invariance in the x axis. Firstly we notice that time evolution with $\hat{H}_{\rm P}$ preserves the parity $\pi(n,s)=e^{i\pi n_s}$ of the state $|n,s\rangle$, with $n_s=n+(s+1)/2$. That is, the parity operator $\hat{\Pi}=e^{i\pi\hat{n}_\sigma}$, with $\hat{n}_\sigma=\hat{n}+(\sigma_z+\sigma_0)/2$, commutes with $\hat{H}_{\rm P}$. Therefore, both operators can then be jointly diagonalized. This means that the matrix elements $\langle n,s|\hat{H}_{\rm P}|n',s'\rangle\propto\delta_{\pi(n,s),\pi(n',s')}$ are zero between states of different parity. This parity symmetry helps in the diagonalization process. Indeed, any (non-degenerate) eigenstate of $\hat{H}_{\rm P}$ has a definite parity. We shall denote by

$$|\psi_k\rangle=\sum_{n,s}c_{n,s}^{(k)}|n,s\rangle \tag{8}$$

the Hamiltonian eigenstates with LL index $k\in\mathbb{Z}$ ($k>0$ for conduction and $k<0$ for valence band). The sum $\sum_{n,s}$ is constrained to $\pi(n,s)=\pm1$, depending on the even (+) and odd (−) parity of k. The coefficients $c_{n,s}^{(k)}$ are obtained by numerical diagonalization of the Hamiltonian matrix, which is truncated to $n\leq N$, with N large enough to achieve convergent results for given values of the magnetic and electric fields. In order to study the effect of a band inversion (topological phase transition), we shall consider electric potentials around $\Delta\simeq-E_g=-1.52$eV, more precisely, we shall analyze the window $-1.9\leq\Delta\leq-1.0$. For a magnetic field of $B=20$T, convergence is achieved for $N=210$ states inside the range $-1.9\leq\Delta\leq-1.0$. We have seen that N must grow with $|\Delta|$ for $\Delta<-1.9$ (TI region) in order to achieve convergence. Similar qualitative results are obtained for lower values of the magnetic field.

In Figure 2 we represent the electronic band structure of phosphorene and silicene as a function of the electric potential Δ. We select the first 13 low energy LLs $k=-6,\ldots,0,\ldots,6$: 6 valence states (even and odd), 6 conduction states (even and odd) and the edge state $k=0$ (black solid line). The edge state $k=0$ undergoes a band inversion around the critical value of the electric potential $\Delta_c=-E_g$ for phosphorene and $\Delta_c=-\Delta_{\rm so}$ for silicene, for which a topological transition occurs from a band-insulator (BI) phase ($\Delta>\Delta_c$) to a topological insulator (TI) phase ($\Delta<\Delta_c$).

Note that the diagonalization of the Hamiltonian $\hat{H}_{\rm S}$ in (7) for silicene is much easier and can be done analytically. This is due to a larger symmetry which makes the model integrable. Indeed, not only the parity $\hat{\Pi}=e^{i\pi\hat{n}_\sigma}$, but also the "total number of excitations" $\hat{n}_\sigma=\hat{n}+(\sigma_z+\sigma_0)/2$, commute with $\hat{H}_{\rm S}$. Therefore, $\hat{H}_{\rm S}$ and $\hat{n}_\sigma$ can be jointly diagonalized, the corresponding Hamiltonian eigenvalues being [49–52]

$$E_n=\begin{cases}\mathrm{sgn}(n)\sqrt{|n|\hbar^2\omega^2+\Delta_g^2}, & n\neq0,\\ -\Delta_g, & n=0,\end{cases} \tag{9}$$

and the Hamiltonian eigenvectors

$$|\psi_n\rangle=-ic_{n+}||n|-1,1\rangle+c_{n-}||n|,-1\rangle, \tag{10}$$

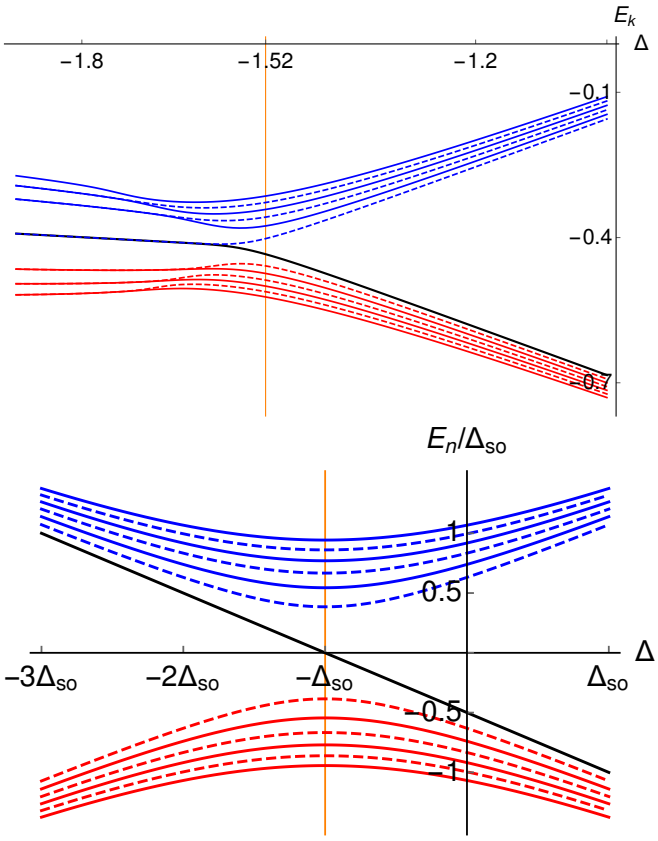

FIG. 2: Low energy spectra E_k of phosphorene (top panel, in eV units) and silicene (bottom panel, in $\Delta_{\rm so}=4$meV units) as function of the electric field strength Δ for 13 LLs $k=-6,\ldots,0,\ldots,6$ ($B=20$T for phosphorene and $B=0.5$T for silicene). Valence (conduction) band LLs $k=-6,\ldots,-1$ ($k=1,\ldots,6$) are represented in red (blue) color (solid for even and dashed for odd parity). The edge state $k=0$, represented in solid black, suffers band inversion around the critical electric potential $\Delta_c=-1.52$eV for phosphorene and $\Delta_c=-\Delta_{\rm so}$ for silicene (these transition points are marked with a vertical orange gridline). Even and odd parity LLs for phosphorene degenerate in the topological insulator region, in particular, the edge state degenerates with the odd parity conduction band LL $k=1$ for $\Delta<\Delta_c$.

with coefficients

$$c_{n+} = \mathrm{sgn}(n)\sqrt{\frac{|E_n|+\mathrm{sgn}(n)\Delta_g}{2|E_n|}}, \quad n\neq 0, \quad (11)$$

$$c_{n-} = \sqrt{\frac{|E_n|-\mathrm{sgn}(n)\Delta_g}{2|E_n|}}, \quad n\neq 0, \quad (12)$$

and $c_{0+}=0$, $c_{0-}=1$ for the edge state.

Let us have a closer look to the structure of these first low energy LLs. Actually, we shall restrict ourselves to the even parity conduction $k=6$ (solid blue) and valence $k=-6$ (solid red) eigenstates, together with the edge state $k=0$ (solid black), since odd states display a similar behavior. We shall visualize the structure of these LLs in phase space, making use of the coherent state representation of $|\psi_k\rangle$, that is, the Husimi distribution function, and its moments, which turn out to be good markers of the BI-TI transition.

IV. COHERENT STATES, HUSIMI FUNCTION AND REDUCED DENSITY MATRICES

Coherent states are usually obtained by applying a displacement operator (a unitary operation) on a highest/lowest weight state, namely $|n\rangle\otimes|s\rangle = |0\rangle\otimes|-\rangle$. We have two kinds of coherent states associated to each sector. One is related to the oscillator or Landau sector

$$|\alpha\rangle = e^{\alpha a^\dagger - \bar\alpha a}|0\rangle = e^{-|\alpha|^2/2}\sum_{n=0}^{\infty}\frac{\alpha^n}{\sqrt{n!}}|n\rangle, \quad (13)$$

where $\alpha = q+ip$ is a complex number. The other is related to the band (spin) sector

$$|\theta,\phi\rangle = e^{\frac{\theta}{2}(e^{i\phi}\sigma_+ - e^{-i\phi}\sigma_-)}|-\rangle = \cos\frac{\theta}{2}|-\rangle + e^{i\phi}\sin\frac{\theta}{2}|+\rangle, \quad (14)$$

where $\sigma_\pm = \frac{1}{2}(\sigma_x \pm i\sigma_y)$, and (θ,ϕ) are the polar and azimuthal angles on the Bloch sphere. These are the usual spin-$\frac{1}{2}$ SU(2) coherent states (the N-band case would require $SU(N)$ coherent states, in principle).

It is well known (see e.g. [53]) that coherent states form an overcomplete set of the corresponding Hilbert space and fulfill the closure relations or resolutions of the identity:

$$1_{\mathrm{L}} = \frac{1}{\pi}\int_{\mathbb{R}^2} d^2\alpha|\alpha\rangle\langle\alpha|, \; d^2\alpha = dqdp, \quad (15)$$

$$1_{\mathrm{B}} = \frac{1}{2\pi}\int_R \sin\theta d\theta d\phi|\theta,\phi\rangle\langle\theta,\phi|, \; R=[0,\pi]\times[0,2\pi],$$

in the Landau (L) and band (B) sectors, respectively. The coherent state, or phase space, representation of a basis state $|n,s\rangle$ is then given by:

$$\varphi_{n,s}(\alpha;\theta,\phi) = \langle n|\alpha\rangle\langle s|\theta,\phi\rangle = \frac{e^{-\frac{|\alpha|^2}{2}}\alpha^n}{\sqrt{n!}}\frac{(\tan\frac{\theta}{2}e^{i\phi})^{\frac{1+s}{2}}}{\sec\frac{\theta}{2}}. \quad (16)$$

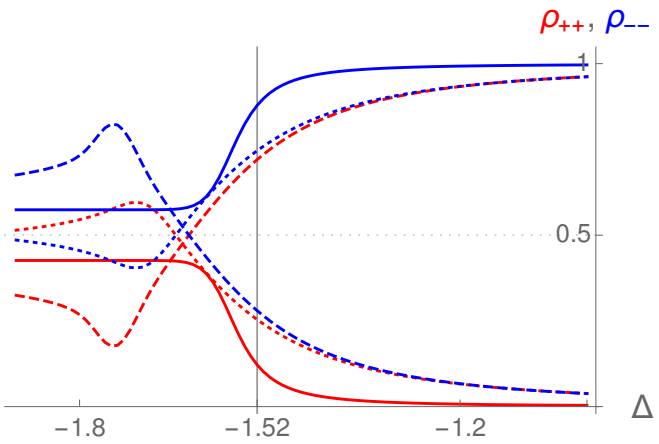

FIG. 3: Diagonal components ϱ_{++} (red) and ϱ_{--} (blue) of the reduced density matrix ($\rho^{\mathrm{B}}_{\psi_k}$), for three Landau levels $k=-6$ (valence band, dotted), $k=0$ (edge state, solid) and $k=6$ (conduction band, dashed), as a function of the electric potential Δ. The critical point $\Delta_c = -1.52$eV, separating the band ($\Delta>\Delta_c$) from the topological insulator ($\Delta<\Delta_c$) regime, is marked with a vertical grid line.

The Husimi or Q-function of a normalized state $|\psi_k\rangle$ like (8) is defined as

$$Q_{\psi_k}(\alpha;\theta,\phi) = |\langle\alpha;\theta,\phi|\psi_k\rangle|^2 = \sum_{n,n'}\sum_{s,s'} c^{(k)}_{ns}\bar c^{(k)}_{n's'}\varphi_{n,s}(\alpha;\theta,\phi)\bar\varphi_{n',s'}(\alpha;\theta,\phi), \quad (17)$$

and normalized according to:

$$\int_{\mathbb{R}^2\times R} Q_{\psi_k}(\alpha,\theta,\phi)\frac{d^2\alpha\sin\theta d\theta d\phi}{2\pi^2} = 1. \quad (18)$$

We are interested in visualizing the Landau and band sectors separately. Therefore, we shall define the reduced density matrices of the Landau sector

$$\rho^{\mathrm{L}}_{\psi_k} = \sum_{n,\bar n}\sum_s c^{(k)}_{ns}\bar c^{(k)}_{\bar n s}|n\rangle\langle\bar n| \quad (19)$$

and of the band sector

$$(\rho^{\mathrm{B}}_{\psi_k}) = \begin{pmatrix}\varrho_{++} & \varrho_{+-}\\ \varrho_{-+} & \varrho_{--}\end{pmatrix} = \begin{pmatrix}\sum_n |c^{(k)}_{n+}|^2 & \sum_n c^{(k)}_{n+}\bar c^{(k)}_{n-}\\ \sum_n \bar c^{(k)}_{n+}c^{(k)}_{n-} & \sum_n |c^{(k)}_{n-}|^2\end{pmatrix}. \quad (20)$$

Parity symmetry implies that $\varrho_{-+}=\varrho_{-+}=0$. In figure 3 we plot the populations ϱ_{++} and ϱ_{--} of three Landau levels $k=-6,0,6$ as a function of the electric potential Δ. The plot reflects the fact that $\varrho_{++}+\varrho_{--}=1$ and therefore they are symmetric respect to the value 1/2. In the BI region ($\Delta\gg -1.52$eV) the band populations of Hamiltonian eigenstates are polarized: $\varrho_{--}\simeq 1$ for edge and valence band and $\varrho_{++}\simeq 1$ for conduction band states; whereas in the TI region ($\Delta\ll -1.52$eV) we have $\varrho_{--}\simeq\varrho_{++}$ (balanced populations).

We are also interested in visualizing the corresponding "marginal" or reduced Husimi functions $Q^{\rm L}_{\psi_k}(\alpha) = \langle\alpha|\rho^{\rm L}_{\psi_k}|\alpha\rangle$ and $Q^{\rm B}_{\psi_k}(\theta,\phi) = \langle\theta,\phi|\rho^{\rm B}_{\psi_k}|\theta,\phi\rangle$, respectively. In Figure 4, the phase-space behavior of the Landau levels is exhibited by the Husimi function $Q^{\rm L}_{\psi_k}(\alpha)$. One can see a transition from a bimodal regime to a unimodal regime. Also, from the BI to the TI phases, there is a continuous delocalization of the Landau levels in phase space. We see in Figure 4 that the edge state $k = 0$ displays a "Schödinger cat structure" structure, that is, a quantum superposition of quasiclassical, macroscopically distinguishable (no overlapping) states (also called "parity-adapted coherent states"). This structure is shared by the ground state of atom-field systems in the superradiant phase, as we show in section VI. This delocalization property is quantified later on Figure 6 by using the Husimi function second moment.

In Figure 5, we represent $Q^{\rm B}_{\psi_k}(\theta,\phi)$ which, for Hamiltonian eigenvalues with defined parity, turns out to be independent of ϕ. We find that $Q^B_0(\theta) \simeq 0.5$ in the TI region, that is, the Husimi band distribution of the edge state is quite uniform between the north ($\theta = 0$) and the south ($\theta = \pi$) poles of the Bloch sphere. This is consistent with Figure 3, where we found that $\varrho_{--} \simeq \varrho_{++}$ (balanced populations) for the edge state in the TI region. The analysis $Q^B(\theta)$ for the BI phase, and for the valence and conduction states, is also consistent with the results of the band populations in Figure 3.

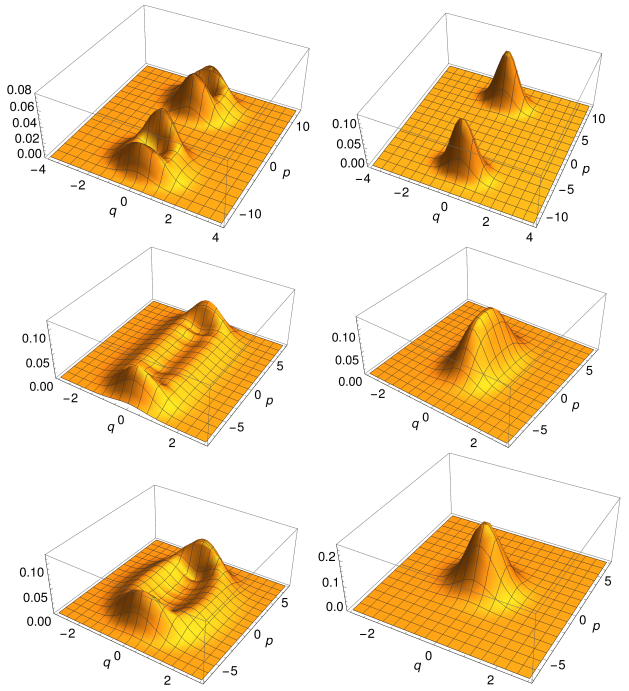

FIG. 4: (Color online) 3D-Plot of the reduced Husimi distribution $Q^{\rm L}_{\psi_k}(\alpha)$, as a function of $\alpha = q + ip$, for the edge state $k = 0$ (right column) and the even-parity valence-band state $k = -6$ (left column), for different values of the electric potential Δ (from top to bottom): $\Delta = -1.8$ (topological-insulator region), $\Delta = -1.52$ (critical) and $\Delta = -1$ (band-insulator region).

V. INFORMATION MEASURES OF ENERGY EIGENSTATES AND BI-TI TRANSITION

We have visualized the structure in phase space of the reduced density matrices $\rho^{\rm L}_{\psi_k}$ and $\rho^{\rm B}_{\psi_k}$ across the critical point Δ_c, noticing a higher delocalization of the corresponding Husimi distributions in the TI phase. Now we want to quantify this delocalization by using the ν-th moments of the reduced Husimi distributions of a state ψ

$$M^{L,\nu}_{\psi} = \int_{\mathbb{R}^2} \frac{d^2\alpha}{\pi} Q^{\rm L}_{\psi}(\alpha)^{\nu}, \qquad (21)$$
$$M^{B,\nu}_{\psi} = \int_{R} \frac{\sin\theta d\theta d\phi}{2\pi} Q^{\rm B}_{\psi}(\theta,\phi)^{\nu}.$$

When $\psi = \psi_k$ is a Hamiltonian eigenstate, then the moments acquire an intrinsic dependence on the electric potential $M^{L(B),\nu}_{\psi_k}(\Delta)$ and will play the role of an order parameter for the topological phase transition occurring at $\Delta_c = -E_g = -1.52$eV, from the BI $\Delta > \Delta_c$ to the TI $\Delta < \Delta_c$ regime. The definition of the moment is not restricted to integer values of ν. Once $M^{L(B),\nu}_{\psi}$ are known for all integers ν, there is a unique analytic extension to complex (and therefore real) ν. The "classical" (versus quantum von Neumann) Rényi-Wehrl entropy is then defined as:

$$W^{L(B),\nu}_{\psi} = \frac{1}{1-\nu}\ln(M^{L(B),\nu}_{\psi}), \qquad (22)$$

which tends to the Wehrl entropy

$$W^{L(B)}_{\psi} = -\int d\mu^{L(B)}\, Q^{L(B)}_{\psi} \ln Q^{L(B)}_{\psi} \qquad (23)$$

when $\nu \to 1$, where $d\mu^L = d^2\alpha/\pi$ and $d\mu^B = \sin\theta d\theta d\phi/(2\pi)$. Among all moments we shall single-out the so-called "inverse participation ratio" (IPR) $M^{L(B),2}_{\psi}$, which somehow measures the inverse of the area (localization) occupied by $Q^{L(B)}_{\psi}$ in phase space. It is also related to the purity $P = {\rm tr}(\rho^2)$ (the trace of the squared reduced density matrix) of the state and measures how entangled they are the band (B) and the Landau (L) sectors across the topological phase transition. The purity is related to the linear entropy by $S = 1 - P$. The maximum values of $M^{L,2}_{\rm max} = \frac{1}{2}$ and $M^{B,2}_{\rm max} = \frac{2}{3}$ are attained when $|\psi\rangle$ is itself a coherent state $|\alpha'; \theta', \phi'\rangle$ (minimal area). This is related to the Wehrl-Lieb's conjecture [54, 55]. For the sake of convenience, we shall normalize the second moments in the Landau and band sectors according to $P^L_{\psi} \equiv 2M^{L,2}_{\psi}$ and $P^B_{\psi} \equiv \frac{3}{2}M^{B,2}_{\psi}$, respectively, in order to set the maximum IPR values to 1 in both sectors. Performing the integrals (21) for a Hamiltonian eigenstate

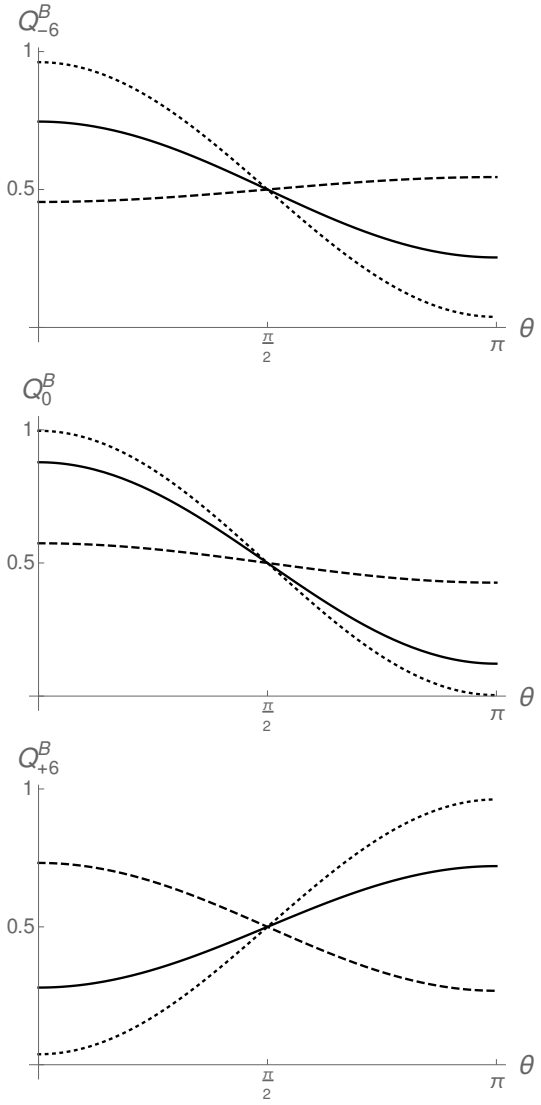

FIG. 5: Reduced Husimi distribution $Q^{\rm B}_{\psi_k}(\theta)$, for the valence-band state $k=-6$ the edge state $k=0$ and the conduction-band state $k=+6$, for different values of the electric potential: $\Delta=-1.8$ (topologial-insulator region, dashed line), $\Delta=-1.52$ (critical point, solid line) and $\Delta=-1$ (band insulator region, dotted line).

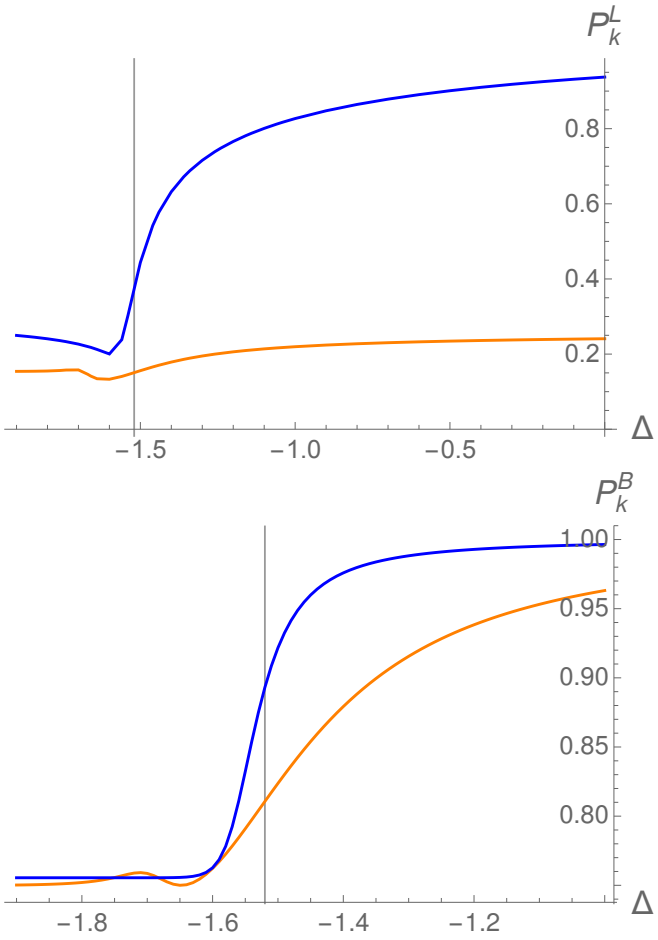

FIG. 6: Normalized inverse participation ratios (IPR) P^L_k and P^B_k as function of the electric potential strength Δ for the edge state $k=0$ (in blue) and the even-parity valence-band state $k=-6$ (in orange). The critical point $\Delta_c=-1.52$eV, separating the band from the topological insulator regime, is marked with a vertical grid line.

(8), we arrive to the explicit formula for the normalized IPR in the Landau sector

$$P^L_k=\sum_{\substack{n,\,\bar n\\ n',\,\bar n'}}\sum_{s,s'}\frac{(n+n')!c^{(k)}_{ns}\bar c^{(k)}_{\bar n s}c^{(k)}_{n's'}\bar c^{(k)}_{\bar n's'}}{2^{n+n'}(n!\bar n!n'!\bar n'!)^{1/2}}\delta_{n+n',\bar n+\bar n'} \tag{24}$$

and in the band sector

$$P^B_k=\varrho^2_{++}+\varrho^2_{--}+\varrho_{++}\varrho_{--}+|\varrho_{+-}|^2 \tag{25}$$

where $\varrho_{\pm\pm}$ are the components of $(\rho^{\rm B}_{\psi_k})$ in (20). In Figure 6 we plot P^L_k and P^B_k as function of the electric potential strength Δ. Notice that the maximum delocalization (minimal IPR, high entanglement) of the energy eigenvectors in phase-space occurs in the TI phase ($\Delta<-1.52$eV), whereas in the BI phase ($\Delta<-1.52$eV) the corresponding wave functions are highly localized (maximum IPR, low entanglement). This behavior is also shared with silicene [34, 36]. In fact, delocalization and entanglement in phase space turns out to be a common feature also of QPTs [32]. In fact, in the next section we analyze the phase space structure of normal and superradiant phases of two paradigmatic spin-boson systems (Rabi-Dicke and Jaynes-Cummings), comparing with band and topological insulator phases of phosphorene and silicene, respectively.

VI. COMPARISON WITH RABI-DICKE AND JAYNES-CUMMINGS MODELS

In this section we want to highlight some analogies between topological insulator and superradiant quantum phases. To this end, we shall discuss on some similarities between the effective Hamiltonian (5,6) for phosphorene and the well known Rabi-Dicke Hamiltonian

$$\hat{H}_{\rm R} = \hbar\omega_0\frac{\sigma_z}{2} + \hbar\omega\hat{a}^\dagger\hat{a} + \frac{\hbar\Omega}{2}(\hat{a}+\hat{a}^\dagger)(\sigma_+ + \sigma_-), \quad (26)$$

originally introduced in the context of nuclear magnetic spin resonance, but later extended to modeling the interaction (with coupling strength Ω) of a two-level system (spin, atoms, superconducting qubits, etc) of transition frequency ω_0 with an harmonic oscillator (electromagnetic field, resonator, phonons, etc) of cavity frequency ω. As for phosphorene, Rabi-Dicke Hamiltonian also conserves the parity $\pi(n,s) = e^{i\pi n_s}$ of the state $|n,s\rangle$, with $n_s = n + (s+1)/2$, since the parity operator $\hat{\Pi} = e^{i\pi\hat{n}_\sigma}$, with $\hat{n}_\sigma = \hat{n} + (\sigma_z + \sigma_0)/2$, also commutes with $\hat{H}_R$. When quickly oscillating "counter-rotating" terms $\hat{a}^\dagger\sigma_+$ and $\hat{a}\sigma_-$ are ignored ("rotating-wave approximation"), the Rabi-Dicke Hamiltonian becomes the Jaynes-Cummings Hamiltonian

$$\hat{H}_{\rm JC} = \hbar\omega_0\frac{\sigma_z}{2} + \hbar\omega\hat{a}^\dagger\hat{a} + \frac{\hbar\Omega}{2}(\hat{a}\sigma_+ + \hat{a}^\dagger\sigma_-), \quad (27)$$

which now also conserves the number of excitations $\hat{n}_\sigma = \hat{n} + (\sigma_z + \sigma_0)/2$, and not only the parity $\hat{\Pi}$, just like the silicene Hamiltonian (7) does. This conservation law leads to a U(1)-continuous symmetry. As for silicene, this case is far simpler, and the diagonalization can be done in the subspaces $\mathcal{H}_n = \{|n,1\rangle, |n+1,-1\rangle\}$, the energy eigenvalues being

$$E_n^\pm = \hbar\omega(n+\frac{1}{2}) \pm \frac{1}{2}\hbar\sqrt{\delta^2 + \Omega^2(n+1)}, \quad (28)$$

where $\delta = \omega_0 - \omega$ is the detuning parameter. The Hamiltonian eigenstates are

$$|\psi_n^\pm\rangle = \cos\frac{\varphi_n}{2}|n+\frac{1\mp1}{2}, \pm1\rangle \pm \sin\frac{\varphi_n}{2}|n+\frac{1\pm1}{2}, \mp1\rangle, \quad (29)$$

where $\varphi_n = \arctan\frac{\Omega\sqrt{n+1}}{\delta}$. Note the similarities between this case and the silicene Hamiltonian eigenvalues (9) and eigenstates (10), although here n is restricted to non-negative numbers, $n \geq 0$, due to the presence of $\hbar\omega\hat{a}^\dagger\hat{a}$ in the Hamiltonian.

When we have an ensemble of N identical two-level atoms, the Rabi-Dicke Hamiltonian becomes the Dicke Hamiltonian by replacing $\sigma_\pm \to J_\pm/\sqrt{N}$, where $J_\pm$ are angular momentum ladder operators for a pseudospin $j = N/2$. In the thermodynamic limit $N \to \infty$, and at a critical value $\Omega_c = \sqrt{\omega_0\omega}$ of the atom-field coupling strength Ω, this system undergoes a quantum phase transition from a normal ($\Omega < \Omega_c$) to a superradiant ($\Omega > \Omega_c$) phase. For finite values of N we still can observe precursors of this quantum phase transition.

Our two-band model of phosphorene shares many similarities with the Dicke model for $N = 1$, $j = 1/2$ (i.e. the Rabi-Dicke model). Actually, there is a parallelism between the TI phase of phosphorene and the superradiant phase of the atom-field system. In fact, the phase space structure of edge states turns out to be similar to the ground state structure of the atom-field system across the critical point. Coherent states prove to be an excellent variational approximation of the ground state in QPTs. Let us denote for simplicity $|z\rangle = |\theta,\phi\rangle$, $z = \tan(\theta/2)e^{i\phi}$ the coherent state (14). Using the direct product $|\alpha, z\rangle \equiv |\alpha\rangle\otimes|z\rangle$ as a ground-state ansatz for the Rabi-Dicke Hamiltonian (26), one can easily compute the mean energy

$$\begin{aligned}\mathcal{H}(\alpha,z) &= \langle\alpha,z|H|\alpha,z\rangle \\ &= \omega|\alpha|^2 + j\omega_0\tfrac{|z|^2-1}{|z|^2+1} + \Omega(\alpha+\bar{\alpha})\tfrac{\bar{z}+z}{|z|^2+1},\end{aligned} \quad (30)$$

which defines a four-dimensional "energy surface". Minimizing with respect to these four (two complex z, α) coordinates gives the equilibrium points:

$$\begin{aligned}\alpha_0 &= \begin{cases} 0, & \text{if } \Omega < \Omega_c, \\ -\sqrt{\frac{\omega_0}{\omega}}\frac{1}{\Omega\Omega_c}\sqrt{\Omega^4 - \Omega_c^4}, & \text{if } \Omega \geq \Omega_c \end{cases} \\ z_0 &= \begin{cases} 0, & \text{if } \Omega < \Omega_c, \\ \sqrt{\frac{\Omega^2-\Omega_c^2}{\Omega^2+\Omega_c^2}}, & \text{if } \Omega \geq \Omega_c, \end{cases}\end{aligned} \quad (31)$$

together with $-\alpha_0$ and $-z_0$. Note that α_0 and z_0 are real and non-zero above the critical point Ω_c (i.e., in the superradiant phase). The existence of two solutions, (α_0, z_0) and $(-\alpha_0, -z_0)$ indicates that the ground state is degenerate in the superradiant phase. This is related to the parity symmetry $\hat{\Pi}$ of the Hamiltonian (26). Therefore, the variational approximation to the ground state is a (even) parity-adapted coherent state

$$|\psi_0\rangle = \frac{|\alpha_0\rangle\otimes|z_0\rangle + |-\alpha_0\rangle\otimes|-z_0\rangle}{\mathcal{N}(\alpha_0, z_0)}, \quad (32)$$

where

$$\mathcal{N}(\alpha_0, z_0) = \sqrt{2}\left(1 + e^{-2|\alpha_0|^2}\left(\frac{1-|z_0|^2}{1+|z_0|^2}\right)^{2j}\right)^{1/2} \quad (33)$$

is a normalization factor. This parity-adapted coherent state is also called a "Schrödinger's cat state" in the literature, in the sense that it is a quantum superposition of two quasi-classical, macroscopically distinguishable states [56].

Taking into account the coherent state overlaps

$$\begin{aligned}\langle\alpha| \pm \alpha_0\rangle &= e^{-\frac{1}{2}|\alpha| - \frac{1}{2}\alpha_0^2 \pm \bar{\alpha}\alpha_0}, \\ \langle z| \pm z_0\rangle &= \frac{(1 \pm \bar{z}z_0)^{2j}}{(1+|z|^2)^j(1+z_0^2)^j},\end{aligned} \quad (34)$$

the Husimi function for the variational ground state states (32), $Q_0(\alpha, z) = |\langle \alpha, z|\psi_0\rangle|^2$, can be simply written as:

$$Q_0(\alpha, z) = \frac{|\langle\alpha|\alpha_0\rangle\langle z|z_0\rangle + \langle\alpha| - \alpha_0\rangle\langle z| - z_0\rangle|^2}{\mathcal{N}^2(\alpha_0, z_0)}. \quad (35)$$

A plot of this function in the normal ($\Omega < \Omega_c$) and superradiant ($\Omega < \Omega_c$) phases and at the critical point ($\Omega = \Omega_c$) can be seen in Ref. [20]. One can appreciate the similarities between this Husimi function and the reduced Husimi distribution $Q_0^L(\alpha)$ of the edge state in Figure 4 (right panel). The normal phase of the matter-radiation system ($\Omega < \Omega_c$) corresponds to the band-insulator phase ($\Delta > \Delta_c$), where the Husimi distribution is highly localized (a single hump), whereas the superradiant phase of the atom-field system ($\Omega > \Omega_c$) corresponds to the topological-insulator phase ($\Delta < \Delta_c$), where the Husimi distribution is delocalized (two humps), displaying a Schrödinger cat structure.

The role of Landau and band sectors in 2D Dirac materials is now played by the field and the atom sectors in the spin-boson system. Refs. [57–60] consider the entanglement between the atoms and the field in the ground state of the Dicke model, showing that the entanglement sharply grows in the superradiant phase. In this sense, we also observe a clear analogy between the topological insulator and the superradiant phases. Indeed, in Figure 6 we represent the purity of the reduced density matrices in the band and Landau sectors for the edge state, which shows that the edge state is far more entangled in the topological than in the band insulator phase. This reinforces the analogy between topological insulator and superradiant phases.

VII. CONCLUSIONS

We have analyzed the low energy regime of two 2D Dirac materials like phosphorene and silicene under the influence of external perpendicular magnetic and electric fields. The electric field is used to tune the band gap (Dirac mass) and to control the appearance of edge currents in the topological insulator phase. We visualize the structure of the edge and first Landau levels using different information-theoretic measures, as a function of the electric field in the vicinity of the topological phase transition. In particular, we use a representation of edge and first LL states in terms of coherent states in phase-space (the Husimi function). We show that the entanglement between the band and Landau sectors is much higher in the topological insulator phase. Under this perspective, we evidence a close analogy between the topological insulator phase of 2D Dirac materials (in particular, phosphorene and silicene) and the superradiant phase of atom-field interaction systems (in particular, the Rabi-Dicke and Jaynes-Cummings models).

This approach offers a new vision that could be extrapolated to general topological insulators and spin-boson systems.

Acknowledgements

M.C. thanks the support of the Spanish Ministry of Science and Universities through the project PGC2018-097831-B-I00. This study has been partially financed by the Consejería de Conocimiento, Investigación y Universidad, Junta de Andalucía and European Regional Development Fund (ERDF), Ref. SOMM17/6105/UGR, the FEDER project UHU-1262561 and the research group FQM-381. O. C. thanks support of the project DGAPA:IN101619.

[1] Sachdev, Subir (2011). Quantum Phase Transitions. Cambridge University Press. (2nd ed.). ISBN 978-0-521-51468-2.
[2] Carr, Lincoln D. (2010). Understanding Quantum Phase Transitions. CRC Press. ISBN 978-1-4398-0251-9.
[3] E.T. Jaynes and F.W. Cummings, Comparison of quantum and semiclassical radiation theories with application to the beam maser, Proc. IEEE. 51, 89-109 (1963). doi:10.1109/PROC.1963.1664.
[4] Andrew D Greentree, Jens Koch and Jonas Larson (Editors), Special issue on Jaynes-Cummings physics, Journal of Physics B, vol. 46, number 22 (2013).
[5] Shun-Qing Shen, Topological Insulators: Dirac Equation in Condensed Matters, 2012 Springer-Verlag Berlin Heidelberg. DOI 10.1007/978-3-642-32858-9.
[6] B.A. Bernevig (with T.L. Hughes), Topological Insulators and Topological Superconductors, 2013 Princeton University Press.
[7] J. K. Asbóth, L. Oroszlány and A. Pályi, A Short Course on Topological Insulators: Band Structure and Edge States in One and Two Dimensions, 2016 Springer International Publishing Switzerland, DOI 10.1007/978-3-319-25607-8.
[8] Michelle J.S. Spencer and Tetsuya Morishita (Eds.), Silicene: Structure, Properties and Applications, Springer Series in Materials Science vol. 235 (2016). DOI: 10.1007/978-3-319-28344-9.
[9] A. Carvalho, M. Wang, X. Zhu, A. S. Rodin, H. Su and A. H. Castro-Neto, Phosphorene: from theory to applications, Nature Review Materials 1, 1-16 (2016).
[10] Wan R, Cao X and Guo J Simulation of Schottky-barrier phosphorene transistors Appl. Phys. Lett. 105, 163511

(2014).
[11] Liu H, Du Y, Deng Y and Ye P D Semiconducting black phosphorus: synthesis, transport properties and electronic applications Chem. Soc. Rev. 44, 2732 (2015).
[12] Akhtar M, Anderson G, Zhao R, Alruqi A, Mroczkowska J E, Sumanasekera G and Jasinski J B Recent advances in synthesis, properties, and applications of phosphorene NPJ 2D Mater. Appl. 1, 5 (2017).
[13] Li, L. et al. Black phosphorus field-effect transistors. Nat. Nanotechnol. 9, 372-377 (2014).
[14] Chen P,Li N,Chen X,Ong W Jand Zhao X, The rising star of 2D black phosphorus beyond graphene: synthesis, properties and electronic applications 2D Mater. 5, 014002 (2017).
[15] Ling X, Wang H, Huang S, Xia F and Dresselhaus M S The renaissance of black phosphorus Proc. Natl Acad. Sci. USA 112, 4523 (2015).
[16] Xu R et al Extraordinarily bound quasi-one- dimensional trions in two-dimensional phosphorene atomic semiconductors ACS Nano 10, 2046 (2016).
[17] E. Romera, M. Calixto and Á. Nagy, Entropic uncertainty and the quantum phase transition in the Dicke model, EPL 97, 20011 (2012).
[18] Calixto, Á. Nagy, I. Paradela and E. Romera, Signatures of quantum fluctuations in the Dicke model by means of Rényi uncertainty, Phys. Rev. A85, 053813 (2012).
[19] E. Romera, R. del Real and M. Calixto, Husimi distribution and phase-space analysis of a Dicke-model quantum phase transition, Phys. Rev. A85, 053831 (2012).
[20] R del Real, M Calixto and E Romera, The Husimi distribution, the Wehrl entropy and the superradiant phase in spin-boson interactions, Phys. Scr. T153, 014016 (2013). doi:10.1088/0031-8949/2013/T153/014016.
[21] M. Calixto, R. del Real, E. Romera, Husimi distribution and phase-space analysis of a vibron-model quantum phase transition, Phys. Rev. A86, 032508 (2012).
[22] M Calixto, E Romera and R del Real, Parity-symmetry-adapted coherent states and entanglement in quantum phase transitions of vibron models, J. Phys. A (Math. & Theor.) 45, 365301 (2012).
[23] M. Calixto and F. Pérez-Bernal, Entanglement in shape phase transitions of coupled molecular benders, Phys. Rev. A 89, 032126 (2014).
[24] E. Romera, M. Calixto and O. Castaños, Phase space analysis of first-, second- and third-order quantum phase transitions in the Lipkin-Meshkov-Glick model, Physica Scripta 89, 095103 (2014).
[25] M. Calixto, O. Castaños and E. Romera, Searching for pairing energies in phase space, EPL 108, 47001 (2014).
[26] M. Calixto, O. Castaños and E. Romera, Entanglement and quantum phase diagrams of symmetric multi-qubit systems, Journal of Statistical Mechanics: Theory and Experiment (2017) 103103.
[27] E. Romera, O. Castaños, M. Calixto and F. Pérez-Bernal, Delocalization properties at isolated avoided crossings in Lipkin-Meshkov-Glick type Hamiltonian models, Journal of Statistical Mechanics: Theory and Experiment (2017) 013101.
[28] C. Pérez-Campos, J.R. González-Alonso, O. Castaños, R. López-Peña, Entanglement and localization of a two-mode Bose-Einstein condensate, Ann. Phys. (NY) 325, 325-344 (2010).
[29] M. Calixto, C. Peón-Nieto and E. Pérez-Romero, Hilbert space and ground-state structure of bilayer quantum Hall systems at $\nu = 2/\lambda$, Phys. Rev. B95, 235302 (2017).
[30] Calixto and C. Peón-Nieto, Husimi function and phase-space analysis of bilayer quantum Hall systems at $\nu = 2/\lambda$, Journal of Statistical Mechanics: Theory and Experiment (2018) 053112.
[31] M. Calixto, C. Peón-Nieto and E. Pérez-Romero, Coherent states for N-component fractional quantum Hall systems and their nonlinear sigma models, Annals of Physics 373, 52-66 (2016).
[32] O. Castaños, M. Calixto, F. Pérez-Bernal and E. Romera, Identifying the order of a quantum phase transition by means of Wehrl entropy in phase space, Phys. Rev. E92, 052106 (2015).
[33] O. Castaños, E. Romera and M. Calixto, Information theoretic analysis of Landau levels in monolayer phosphorene under magnetic and electric fields, Mater. Res. Express 6, 106316 (2019).
[34] M. Calixto and E. Romera, Identifying topological-band insulator transitions in silicene and other 2D gapped Dirac materials by means of Renyi-Wehrl entropy, EPL 109, 40003 (2015).
[35] E. Romera and M. Calixto, Uncertainty relations and topological-band insulator transitions in 2D gapped Dirac materials. Journal of Physics: Condensed Matter 27, 175003 (2015).
[36] M. Calixto and E. Romera, Inverse participation ratio and localization in topological insulator phase transitions, Journal of Statistical Mechanics, P06029 (2015).
[37] E. Romera, M. Calixto, and J. C. Bolívar, Information measures and topological-band insulator transitions in 2D-Dirac materials under external circularly polarized lasers, and static electric and magnetic fields, Physica A 511, 174 (2018).
[38] Corbridge, D. Phosphorus: Chemistry, Biochemistry and Technology 6th edn (CRC Press, 2013).
[39] Bridgman, P. W. Two new modifications of phosphorus. J. Am. Chem. Soc. 36, 1344-1363 (1914).
[40] Bridgman, P. W. Further note on black phosphorus. J. Am. Chem. Soc. 38, 609-612 (1916).
[41] Zhu, Z. and Tománek, D. Semiconducting layered blue phosphorus: a computational study. Phys. Rev. Lett. 112, 176802 (2014).
[42] Guo, H., Lu, N., Dai, J., Wu, X. and Zeng, X. C. Phosphorene nanoribbons, phosphorus nanotubes, and van der Waals multilayers. J. Phys. Chem. C 118, 14051-14059 (2014).
[43] Guan, J., Zhu, Z. and Tománek, D. Phase coexistence and metal-insulator transition in few-layer phosphorene: a computational study. Phys. Rev. Lett. 113, 046804 (2014).
[44] Rodin, A. S., Carvalho, A. and Castro Neto, A. H. Strain- induced gap modification in black phosphorus. Phys. Rev. Lett. 112, 176801 (2014).
[45] Liu, H. et al. Phosphorene: an unexplored 2D semiconductor with a high hole mobility. ACS Nano 8, 4033-4041 (2014).
[46] Rudenko, A. N. and Katsnelson, M. I. Quasiparticle band structure and tight-binding model for single- and bilayer black phosphorus. Phys. Rev. B 89, 201408(R) (2014).
[47] Motohiko Ezawa, Topological origin of quasi-flat edge band in phosphorene, New J. Phys. 16, 115004 (2014).
[48] Zhou, X. Y. et al. Landau levels and magneto-transport property of monolayer phosphorene. Sci. Rep. 5, 12295;

doi: 10.1038/srep12295 (2015).
[49] L. Stille, C. J. Tabert, and E. J. Nicol, Optical signatures of the tunable band gap and valley-spin coupling in silicene, Phys. Rev. B 86, 195405 (2012).
[50] C.J. Tabert and E.J. Nicol, Valley-Spin Polarization in the Magneto-Optical Response of Silicene and Other Similar 2D Crystals, Phys. Rev. Lett. 110, 197402 (2013).
[51] C.J. Tabert and E.J. Nicol, Magneto-optical conductivity of silicene and other buckled honeycomb lattices, Phys. Rev. B 88, 085434 (2013).
[52] M. Tahir, U. Schwingenschlögl, Valley polarized quantum Hall effect and topological insulator phase transitions in silicene, Scientific Reports, 3, 1075 (2013).
[53] A. Perelomov, Generalized Coherent States and Their Applications, Springer-Verlag (1986).
[54] A. Wehrl, Rep. Math. Phys. **16**, 353 (1979).
[55] E.H. Lieb, Commun. Math. Phys. **62**, 35 (1978).
[56] O. Castaños, E. Nahmad-Achar, R. López-Peña, J. G. Hirsch, Superradiant phase in field-matter interactions, Phys. Rev. A 84, 013819 (2011).
[57] N. Lambert, C. Emary, T. Brandes, Entanglement and the Phase Transition in Single-Mode Superradiance, Phys. Rev. Lett. 92, 073602 (2004).
[58] N. Lambert, C. Emary, T. Brandes, Entanglement and Entropy in a Spin-Boson Quantum Phase Transition, Phys. Rev. A 71, 053804 (2005).
[59] O. Castaños, R. López-Peña, E. Nahmad-Achar, J. G. Hirsch, Quantum information approach to the description of quantum phase transitions, J. Phys. :Conf. Ser. 403, 012003 (2012).
[60] O. Castaños, R. López-Peña, E. Nahmad-Achar, J. G. Hirsch, Matter-Field entanglement within the Dicke model, AIP Conf. Proc. 1488, 138 (2012).